Structures 59 (2024) 105796

Contents lists available at ScienceDirect

Structures

journal homepage: www.elsevier.com/locate/structures

Flexural behaviour of GFRP-reinforced concrete pontoon decks under static four-point and uniform loads

Shahrad Ebrahimzadeh [a], Xian Yang [a], Allan Manalo [a], Omar Alajarmeh [a,*], Zaneta Senselova [a], Charles Dean Sorbello [b], Senarath Weerakoon [b], Brahim Benmokrane [c]

[a] Centre for Future Materials (CFM), School of Engineering, University of Southern Queensland, Toowoomba 4350, Australia
[b] Maritime Safety Queensland, Department of Transport and Main Roads, Brisbane, Qld 4000, Australia
[c] University of Sherbrooke, Sherbrooke, Quebec J1K 2R1, Canada

ARTICLE INFO

Keywords:
Cutout
Flexural behaviour
Four-point bending
GFRP bars
Reinforced concrete decks
Uniform distributed loading

ABSTRACT

Concrete pontoon decks are subject to flexural loading actions under concentrated and uniform loads caused by self-weight, live loads, and wave actions. This study investigated the structural behaviour of concrete pontoon decks reinforced with glass fiber-reinforced polymer (GFRP) bars under static four-point and uniform loading conditions. Five large-scale GFRP-reinforced concrete decks with a length of 2400 mm, width of 1500 mm, and thickness of 125 mm were tested to evaluate their moment capacity, strain behaviour, cracking propagation, and failure mechanism. The effects of the loading configurations, reinforcement arrangement, and cutout simulating the piles' location were evaluated. The edge cut-out initiated flexural-shear cracks, causing the pontoon decks to fail at an effective bending stress 10% lower than the solid decks. Decreasing the span-to-depth ratio from 5.6 to 4.0 increased the induced shear stress of a section and caused the deck to fail by shear compression. Uniform loading resulted in an even load distribution and minimized the stress concentration around the cutout. An increase in the effective depth improved all deck flexural characteristics. The equations in ACI 4401. R-15 and CSA S806–12 provided an accurate prediction for solid decks but overestimated the ultimate flexural strength of the GFRP-reinforced concrete decks with a cutout.

Nomenclature

a	Shear span
b	Width of rectangular cross-section
c	Distance from the extreme compression fiber to the neutral axis
d	Distance from the extreme compression fiber to the centroid of the tension reinforcement
d_v	Effective shear depth
E_c	Modulus of elasticity of concrete
E_f	Modulus of elasticity of FRP
E_{fv}	Modulus of elasticity of the FRP shear reinforcement
f'_c	Specified compressive strength
f_f	Stress in the FRP reinforcement under a specified load
f_{fu}	Design tensile strength of FRP, considering reductions for service environment
f_r	Modulus of rupture of concrete
I_g	Gross moment of inertia
k	Neutral-axis factor
K_{el}	Initial stiffness
V_c	Shear strength resistance provided by the concrete
y_t	Distance from the centroidal axis of the cross-section to the extreme fiber in tension
α_1	The ratio of the average stress of the equivalent rectangular stress block to f'_c
β_1	Factor taken as 0.85 for concrete strength up to 28 MPa. Above that, the factor was reduced at a rate of 0.05 for every 7 MPa to a minimum of 0.65
ε_{cu}	Ultimate strain in the concrete
λ	Factor to account for concrete density
ϕ_c	Resistance factor of the concrete
ρ_f	Reinforcement ratio

* Corresponding author.
E-mail address: omar.alajarmeh@usq.edu.au (O. Alajarmeh).

https://doi.org/10.1016/j.istruc.2023.105796
Received 20 August 2023; Received in revised form 30 November 2023; Accepted 19 December 2023
Available online 28 December 2023

1. Introduction

The use of glass fiber-reinforced polymer (GFRP) bars as internal reinforcement for concrete structures is gaining popularity, particularly in constructions located near or on the coast. This trend is primarily driven by the pressing need to counteract the widespread problem of steel-bar corrosion [1]. This escalation in significance can be attributed to the increasing levels of carbon dioxide concentration, temperature, and relative humidity resulting from the impacts of climate change [2]. As a result, many concrete structures designed to have a service life of 100 years have started to deteriorate after only 30 years, costing the Australian government around AUD 8 billion [3]. There is a significant benefit therefore to using alternative reinforcing systems that would eliminate or minimize corrosion problems in reinforced concrete structures.

GFRP rebars are emerging as a reliable and efficient alternative to steel reinforcement in concrete structures situated in corrosive marine environments or aggressive soil conditions and this product offers enhanced performance and reduced maintenance costs compared to steel bars in such challenging environments. Furthermore, the cost competitiveness of GFRP bars is increasing, owing to advancements in fiber and resin materials as well as recent progress in manufacturing techniques [2]. The studies have also demonstrated excellent long-term performance and durability of GFRP bars in aggressive environmental conditions, including high service temperature [4], exposure to seawater [5], high moisture and alkaline environments [6], and highly carbonated chloride environments [7,8]. These studies have confirmed the high-strength properties and strength retention of GFRP bars under aggressive environmental conditions.

Recent studies have investigated the performance of concrete structures and elements internally reinforced with GFRP bars under different loading conditions. It has been found that GFRP-reinforced concrete had superior fatigue performance under cyclic loading simulating the constant exposure of marine concrete structures to tidal current waves [9]. Pioneering experimental and analytical studies demonstrated the benefits of using GFRP bars as internal reinforcement for concrete beams under shear [10] and flexural loading [11,12]. These experimental results combined with the high flexibility and strength of the GFRP bars have resulted in their successful implementation as a precast concrete pocket connection [13], stirrups in self-compacting concrete beams [14], concrete boat-approach [15], and improving the performance of reinforced concrete structures potentially benefits the bridge structures [16,17]. These studies and applications have successfully demonstrated the benefits of the high strength and noncorroding properties of GFRP bars as internal reinforcement for maritime infrastructure.

One marine infrastructure that will benefit from reinforcing with GFRP bars is floating walkway modules, which generally serve as landing decks for boat ramps. Several types of such infrastructure are being replaced due to the corrosion of steel reinforcement, costing the Queensland Department of Transport and Main Roads at least $10 million annually [2]. Moreover, many of these pontoons were damaged in the 2022 Queensland floods, revealing signs of steel corrosion (Fig. 1a). The damage occurred at the corners of the cutout of the pontoon modules due to severe concrete cracking. Cutouts are provided and are necessary in locating the piles used to hold the pontoons in place. These cracks also act as pathways for moisture ingress, resulting in corrosion of the steel reinforcement and localized galvanized corrosion (Fig. 1b). Since preventing concrete cracking is difficult because pontoon decks are continuously subject to various loading actions, the problem of steel corrosion can be eliminated with the use of GFRP bars. A detailed investigation is, however, needed to understand the structural performance of GFRP-reinforced decks with a cutout under different loading configurations representing the conditions that they are subjected to.

This study was implemented to evaluate the flexural performance of concrete pontoon decks reinforced with GFRP bars subject to different loading configurations and with different bar arrangements. The effect of the presence of an edge cutout to simulate the location of the piles was also evaluated. Five large-scale pontoon concrete decks were tested to examine the cracking propagation and failure, strength and stiffness, and strains in the GFRP bars and concrete. The findings from this research will provide a better understanding of the structural behaviour of GFRP-reinforced concrete pontoon decks for their reliable and safe design. It will also increase the confidence and widespread use of GFRP bars for boating, marine, and other critical structures to eliminate the high maintenance and replacement costs because of the steel-corrosion problem.

2. Experimental program

2.1. Characteristics of the material

The precast-concrete pontoon decks were designed according to the Queensland Department of Transport and Main Road's design criteria for floating walkways and pontoons [18] and the Australian standards for concrete structures (AS3600–2018 [19]). Grade III (#3) GFRP bars with a nominal diameter of 10 mm were used to reinforce the concrete pontoon decks (Fig. 2a). The GFRP bars were manufactured with longitudinal EC-R glass fiber yarns impregnated with vinyl-ester resin with a surface sand coating to enhance the bond performance with concrete. Studies [20,21] showed the sand coated bars have good bonding performance with concrete and have higher average bond strength than ribbed-surface GFRP bars. The mechanical properties of the GFRP bars, as determined by [22], and the standard test method followed are listed in Table 1.

(a) Damaged pontoon during the 2022 Queensland flood (Image courtesy of CD Sorbello)

(b) Galvanic corrosion in pontoon decks (Image courtesy of CD Sorbello)

Fig. 1. Different kinds of damage to pontoon decks.

(a) (b)

Fig. 2. (a) #3 GFRP Bars; (b) Cylindrical concrete samples.

Table 1
Properties and test methods of the GFRP bars [22].

Mechanical properties of the bar	Test method	Value
Nominal bar diameter (mm)	CSA S806-2012[37]	10
Nominal bar area (mm^2)	CSA S806-2012[37]	70.8
Ultimate tensile strength (MPa)	ASTM D7205-2011[39]	1315
Modulus of elasticity (GPa)	ASTM D7205-2011[39]	62.5
Ultimate strain (%)	ASTM D7205-2011[39]	2.3

Concrete with a target compressive strength of at least 50 MPa, as recommended in MRTS70 [23] for boating and marine infrastructure in Queensland (Australia), was used. This compressive strength is based on the design concrete mix of S50, which is recommended for durability classification C2 [19]. The cement, water, and aggregates used in the concrete mix complied with (AS3972–2010 [24]), (AS1379–2007 [25]), and (AS 2758.1–2014 [26]) requirements, respectively. The compressive strength of the concrete was evaluated by testing eight cylindrical samples 100 mm in diameter and 200 mm in height (Fig. 2b) at the same time as the testing of the decks (28 days after casting) according to the procedures described in (ASTM C39–2018 [27]). The average compressive strength of the concrete cylinders was 73.4 MPa with a standard deviation of 4.2 MPa.

2.2. Details of the specimens

A total of five large-scale concrete pontoon decks with different arrangements of GFRP bar reinforcement and geometric configurations were manufactured and tested. The overall dimensions of the concrete decks were 2400 mm long, 1500 mm wide, and 125 mm thick. Some decks had a square-edge cutout measuring 300 mm by 300 mm in the middle of the long side of the decks representing the pile location. Pontoon decks are typically manufactured with square cutouts to accommodate the circular piers for practical construction. The edge cutout was produced by inserting a 300 mm by 300 mm piece of Styrofoam inside the formwork before concrete casting. Table 2 presents the description and properties of each specimen, while Fig. 3 depicts the reinforcement dimensions, details, spacing, presence/absence of cutout, and loading conditions.

The specimens listed in Table 2 were designated based on the reinforcing material (G for GFRP bars), bar spacing in mm (150 mm or 250 mm), the number of reinforcing layers (L1 for one layer and L2 for two layers), deck geometry (S for solid or no cutout and C for an edge cutout), and loading type during testing (A for the airbag to apply uniform loads, B for bending under four-point loading, and V for shear testing under four-point loading). For example, specimen G250L2CB is a deck reinforced with GFRP bars spaced at 250 mm on centers arranged in two layers, with an edge cutout, and tested under static four-point loading. The strain in the GFRP bars was measured by attaching electrical-resistance strain gauges with a gauge length of 3 mm to different locations. The details of the dimensions, reinforcement arrangement, concrete cover, spacing, and location of the strain gauges have been demonstrated (Fig. 3). Strain gauges were attached to the GFRP bars between the support and load application (E_1) to identify any potential shear failure. The gauges at the mid-span were to measure both the tensile and compressive strains (C_2, C_3, and C_4) at the location with the highest deformation and bending moment. A uniaxial strain gauge with a length of 20 mm was attached to the topmost concrete surface (SCL).

2.3. Test setup and instrumentation

Various testing configurations were implemented to investigate the structural performance of the GFRP-reinforced concrete pontoon decks. Under uniform loading conditions, two decks (G150L1CA and G250L2CA) were placed over two 950 mm square-shaped airbags to apply pressure beneath them. To create a simply supported slab under uniformly distributed loading, two steel profiles were positioned at the top of the pontoon decks and bolted to fix them to the ground (Fig. 4a). The distance between these steel profiles was set to 2000 mm (Fig. 4b) to match the support-to-support length in the four-point bending test (G250L2CB). The mid-span deflection was measured with a linear variable displacement transducer (LVDT) installed with the load actuator. A laser displacement sensor (LDS) was also positioned beneath the deck in line with the load cell's axis. Using data extracted from LDS, the recorded deflection measured by the LVDT was verified, and the information from it was confidently and correctly used for analysis. All the information—including the applied load, deflection, and strain—was recorded with a System 5000 data logger. A digital image correlation (DIC) system was also employed to monitor deflection along the length on one side of the decks.

In the four-point static bending test (Fig. 5a), the shear span (*a*) between the supports and the loading point was 700 mm (G250L2CB, and G250L2SB), while this distance was decreased to 500 mm for specimen G250L2CV (Fig. 5b). The load was applied through a steel spreader beam using a 2000 kN electro-hydraulic jack with a maximum stroke of 85 mm. The monotonic load was applied in a displacement-control mode at a rate of 5 mm/min rate and was measured using a 500 kN capacity load cell.

3. Results and discussion

This section presents the experimental results (including moment–deflection (Fig. 6), moment–strain, crack propagation, and failure mechanism) from the bending tests of large-scale GFRP-reinforced pontoon concrete decks. It also presents an analysis and discussion on how the investigated design parameters affected the structural behaviour of the GFRP-reinforced concrete pontoon decks.

Table 2
Details of the GFRP-reinforced concrete pontoon deck specimens.

Specimen	Grid spacing (mm)	Reinforcement details	Geometry	Concrete compression strength (MPa)	Standard deviation (MPa)	Loading type
G150L1CA	150	Single layer	Cutout	73.45	4.21	Uniform
G250L2CA	250	Double layer	Cutout	73.45	4.21	Uniform
G250L2CB	250	Double layer	Cutout	73.45	4.21	Bending
G250L2SB	250	Double layer	Solid	73.45	4.21	Bending
G250L2CV	250	Double layer	Cutout	73.45	4.21	Shear

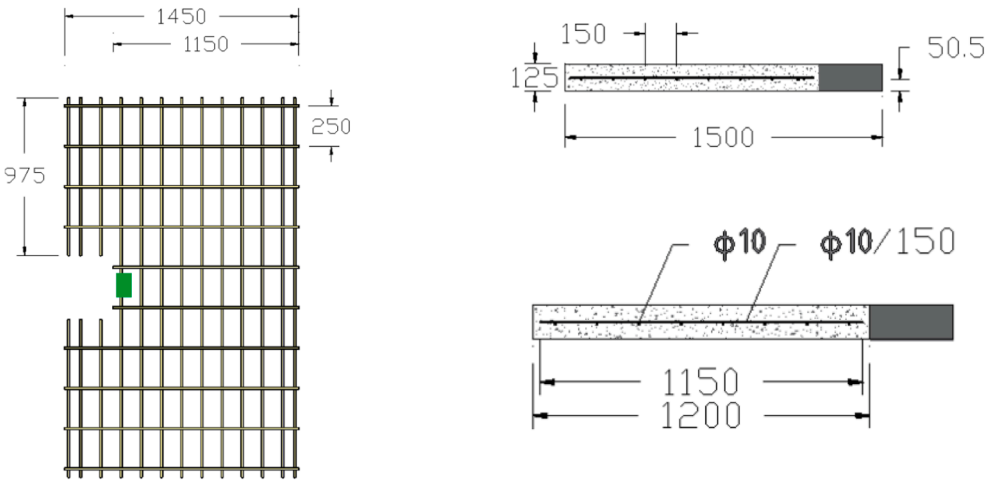

(a) Deck with cutout and reinforced with a single layer of GFRP bars

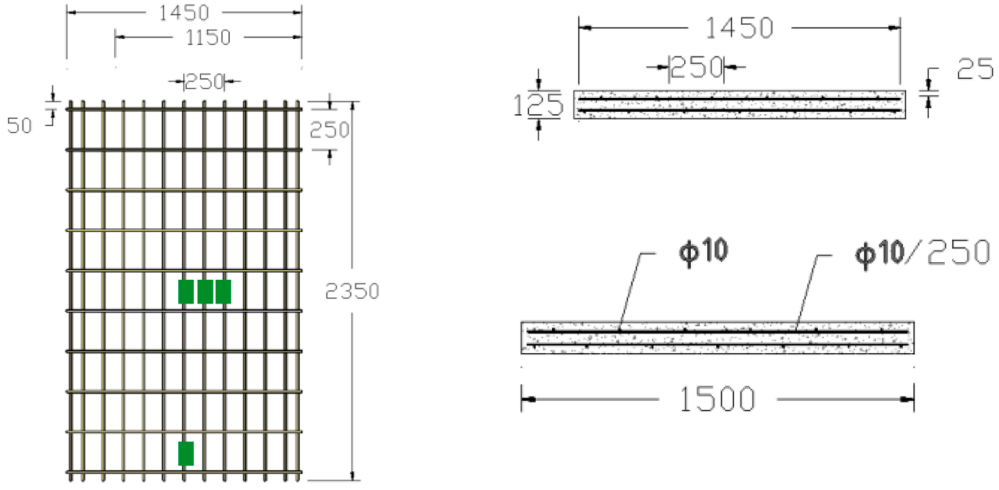

(b) Solid deck reinforced with a double layer of GFRP bars

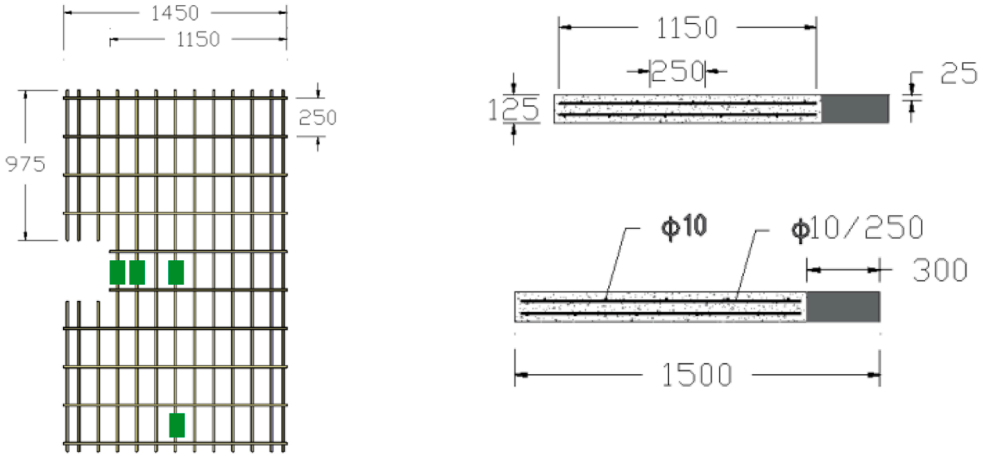

(c) Decks with cutout and reinforced with a double layer of GFRP bars

Fig. 3. Details of the specimens.

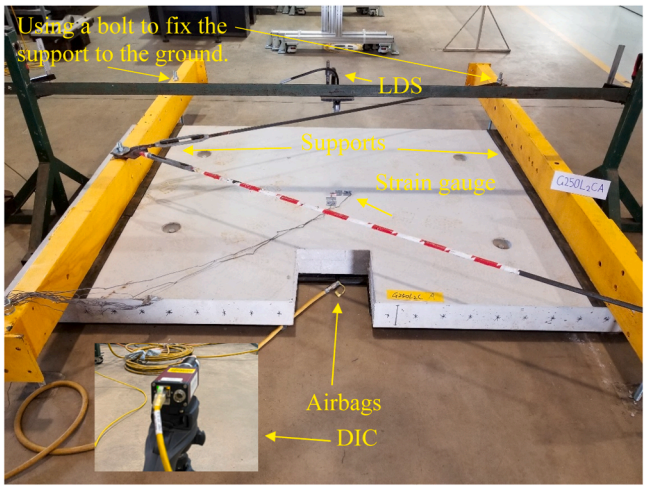

(a) Test setup and instrumentation for the uniform loading test

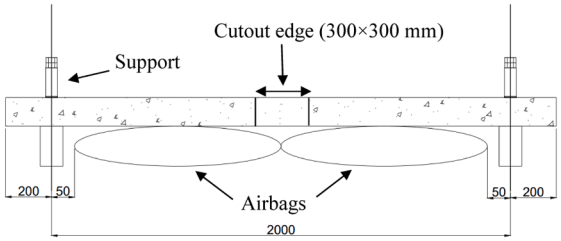

(b) Schematic side view of the uniform loading test

Fig. 4. Test setup for uniform loading.

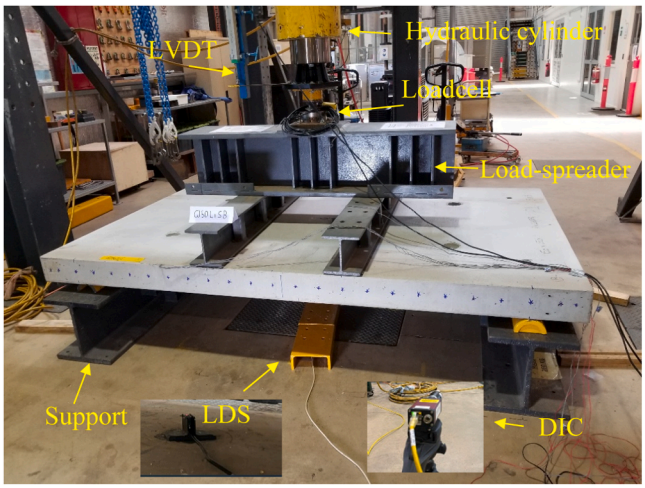

(a) Instrumentation and actual test setup

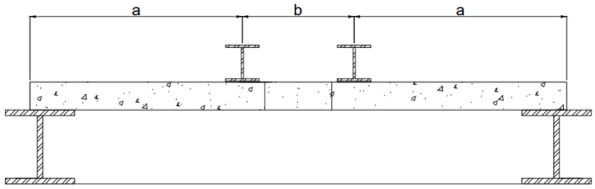

(b) Schematic of the test setup

Fig. 5. Static four-point bending and shear loading test.

Table 3 summarizes the cracking moment, ultimate moment capacity, and the initial stiffness of the tested decks. The initial stiffness (K_{el}) was determined from the slope of the elastic part of the bending moment and deflection curve shown in Fig. 6. Moreover, the failure modes of the decks (F for flexural, CC for concrete compression, F-S for flexural-shear, S-T for shear-tension, and S-C for shear-compression) have been indicated.

3.1. Effect of the edge cutout

3.1.1. Moment capacity and stiffness

The effect of the edge cutout on the flexural behaviour of GFRP-reinforced concrete pontoon decks was evaluated by comparing the behaviour of specimens G250L2SB and G250L2CB. These decks have two layers of reinforcement and were tested under four-point loading. The results indicate that the behaviour of both decks can be divided into two stages. The first is the pre-cracking stage of the concrete wherein both decks behaved in a linear elastic fashion, while the second stage was post-cracking behaviour. Before the initial concrete cracking (first stage), the deck with an edge cutout had a bending stiffness of 9.5 kN/mm, which is 54% lower than that of the solid deck (20.8 kN/mm). Moreover, the deck with a cutout exhibited a 42% lower cracking moment compared to the solid one (G250L2SB). The fact that specimen G250L2CB had lower stiffness and cracking moment than G250L2SB can be mainly attributed to the reduced concrete section as the result of the edge cutout at mid-span and the discontinuity of longitudinal GFRP bars along the length of the deck. This finding agrees with that of Khalil et al. [28] who observed that the initial stiffness for one-way slabs with a rectangular opening in the middle consisting of 16%, 33%, and 50% of the entire width was 39%, 50%, and 66% lower, respectively. The higher percentage reduction in the stiffness and cracking moment of the GFRP-reinforced concrete decks tested in this study is comparable to that of Khalil et al. [28] for the specimen with almost the same reduction in cross-sectional area. This could be due to the cutout located in the edge creating unsymmetrical loading, resulting in a higher stress concentration than the specimens with an opening in the middle.

With the further application of the load, both decks exhibited a nonlinear bending moment and deflection behaviour until the ultimate moment capacities (second stage) were reached. The nonlinear behaviour signifies the widening of the flexural cracks as well as the propagation of the concrete crack along the length of the deck. The deck with an edge cutout then failed at a bending moment of 42.2 kN.m, which is 38% lower than for the solid deck (58.6 kN.m). The fact that specimen G250L2CB had a lower ultimate bending moment capacity than G250L2SB can be attributed to the reduction of the deck's effective width from 1.5 m to 1.2 m at mid-span (20% reduction) and the discontinuity of the longitudinal reinforcement at the edge cutout (30% reduction in the tensile reinforcement ratio). By considering both decks to have a homogenous cross-section and calculating the effective bending stress at mid-span (i.e., $\sigma_b = Mc/I$ where M is the applied bending moment, c is the mid-depth of the section, and I is the uncracked second moment of inertia). As a result, the average bending stress at cracking and failure for the deck with the cutout was 4.22 MPa and 13.5 MPa, respectively, while that of the solid deck was 5.04 MPa and 15 MPa, respectively. The deck with a cutout had a calculated average bending stress at both stages more than 10% lower than the solid deck. This confirms that the sharp corner of the cutout edge initiated the stress concentration. This caused premature concrete cracking at this location, which is described in detail in the section on cracking propagation and failure behaviour. These results and observations demonstrate the impact of the edge cutout on the pre-and post-cracking behaviour of the GFRP-reinforced pontoon decks. Salman [29] compared the effect of the reduction in cross-sectional area as a result of the rectangular opening in the middle of the reinforced concrete one-way slabs under four-point

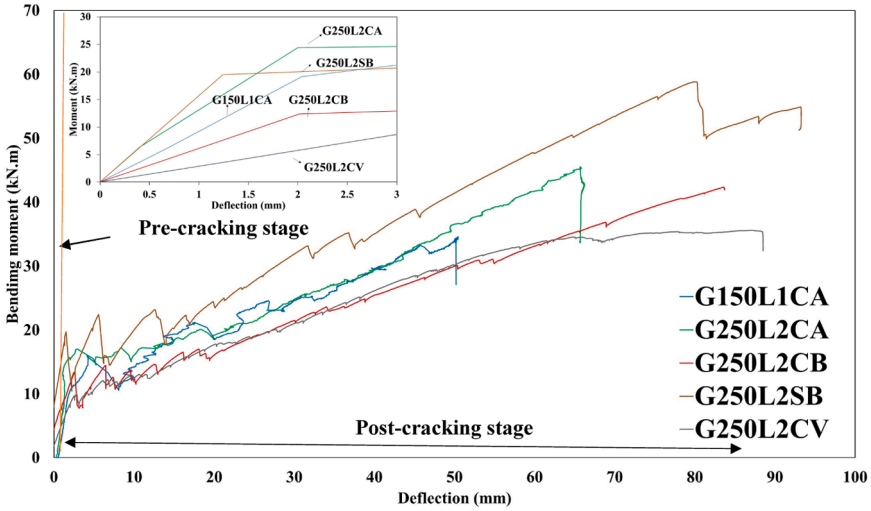

Fig. 6. Moment–deflection behavior.

Table 3
Capacity, stiffness, and ductility results.

Specimen	M_{cr}	(kN.m)	M_u	(kN.m)	K_{el} (kN/mm)	Failure mode	E_{exp} (KJ)	$\Delta_{cr,exp}$ (mm)	$\Delta_{u,exp}$ (mm)	ε_{GFRP} (με)	ε_c (με)
G150L1CA	13.8		37.62		9.47	F-CC	5443	2.43	50.7	5415	-
G250L2CA	19.1		50.6		12.69	F-CC	8508	1.54	66	13644	4341
G250L2CB	13.2		42.24		9.5	F-S	6218	2.7	84.3	12222	3689
G250L2SB	19.7		58.6		20.8	S-T	10309	2.5	94.8	15256	2633
G250L2CV	10.1		33.45		12.8	S-C	9096	3.32	88.9	12798	2872

bending. The results of that study reveal that increasing the area of the opening from 4.2% to 7.4% and 11.6% of the total cross-section decreased the ultimate load capacity of the slab from 36.9 kN to 34.4 kN and 28.2 kN, respectively. The double reduction percentage at the moment capacity compared to the 20% reduction in the cross-sectional area in the current study, represents the double effect compared to that of [29] and can be attributed to the stress concentration generated at the corners of the square edge cutout rather than the existence of the opening in the middle of the deck. The deflection behaviour along the deck length measured with the DIC revealed that the deck with an edge cutout and the solid deck behaved differently. The curves indicate how the cracks developed and progressed along the length (Fig. 7). Since the concrete was still intact in the pre-crack stage, the load and deflection curve along the length of both decks was the same and parabolic in shape. With increasing applied load, the solid deck maintained the parabolic shape of the deflection curve, indicating the section's continuity and uniform distribution of the flexural cracks along the length of the deck (Fig. 7a). As the rotation increased, the concrete cracking propagated through the thickness, reducing the deck's flexural stiffness. In contrast, the deflection along the length of the deck with the edge cutout followed the shape of the bending moment diagram with a constant slope from the support up to the corners of the cutout and a flat slope along the cutout (Fig. 7b). This deflected shape indicates that the corner of the cutout created a discontinuity in the cross-section as the cracking was concentrated heavily at the cutout edges.

3.1.2. *Moment–strain behaviour*

The moment–strain behaviour of the GFRP bars and the concrete in specimens G250L2SB and G250L2CB were analyzed to further evaluate the effect of the edge cutout on the flexural behaviour of the GFRP-reinforced concrete decks. The strains measured in the concrete (SCL), bars in compression (C_2), and in tension (C_3, C_4) increased linearly with the applied bending moment up to 13.2 kN.m and 19.7 kN.m for decks G250L2CB and G250L2SB, respectively (Fig. 8). These bending moment values correspond to the first concrete crack (Table 1). This observation supports the decks' linear elastic moment capacity and deflection behaviour.

After the formation of the first tensile crack in G250L2SB (at 19.7 kN.m), the flexural cracks developed from the mid-span and progressed towards the loading point at 23.7 kN.m. This incident corresponds to the increase of the strain in C_3 and C_4 in the form of the plateau segment. The plateau segment in the strain on the C4 (strain gauge attached to reinforcement in tension) at a bending moment of 19.7 kN.m is due to the formation and widening of the flexural cracks in the mid-span progress towards loading points. This behaviour can be further explained by tensile elongation GFRP bars at the location of the flexural-shear cracks but without increasing capacity in the deck before the failure. Strain gauge E_1 only started to measure strain at 39.7 kN.m. E_1 was attached to the GFRP bar in tension at the shear span of the deck. The strain reading at this location indicates the development of flexural shear cracks near the loading point, which progressed toward the support. At the ultimate bending moment (58.6 kN.m), the strain in the concrete in compression (SCL) was − 1390 $\mu\varepsilon$ while that in E_1 was 3785 $\mu\varepsilon$, and, at the GFRP bars in C_4 where there were widened flexural cracks in C_4, the strain was 15212 $\mu\varepsilon$. The high strain reading in C_4 indicates that the bottom GFRP bars at the location of the flexural-shear cracks stretched significantly before the failure.

When cracks in concrete appeared in the shear span of deck G250L2CB at a bending moment of 30.6 kN.m, a significant increase in strain was measured in the GFRP bars in tension (C_3 and C_4). This can be attributed to the tension bars bridging the concrete and preventing it from widening. The reading at SCL shifted towards zero strain between the applied bending moment of 30.6 kN.m and 42.2 kN.m. This behaviour indicates a significant widening of the concrete crack at the edge cutout, which progressed across the deck's width and divided the deck into three segments. As the concrete in the middle segment was connected to the deck only through the longitudinal GFRP bars, there was no strain measured at this location. On the other hand, C_4 reached

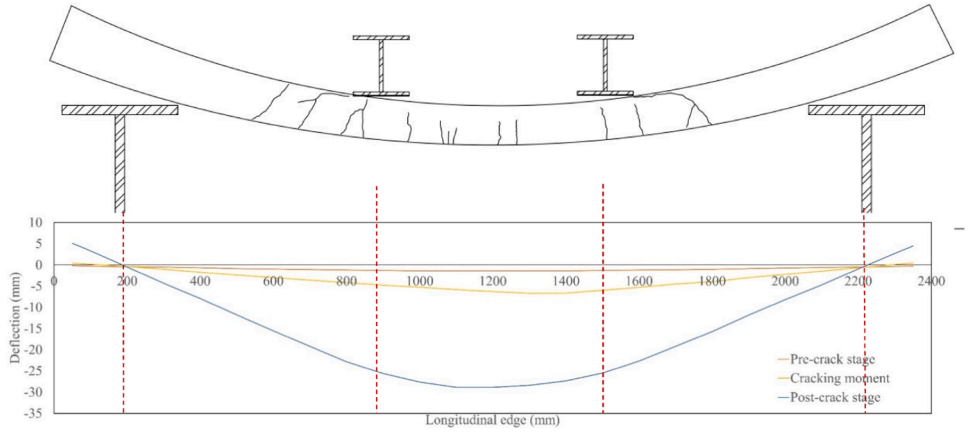

(a) G250L2SB

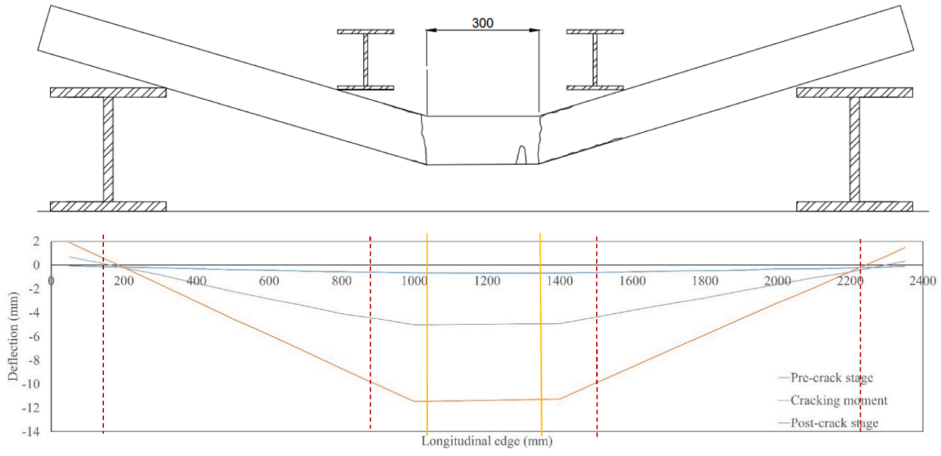

(b) G250L2CB

Fig. 7. Deflection along the length of the deck.

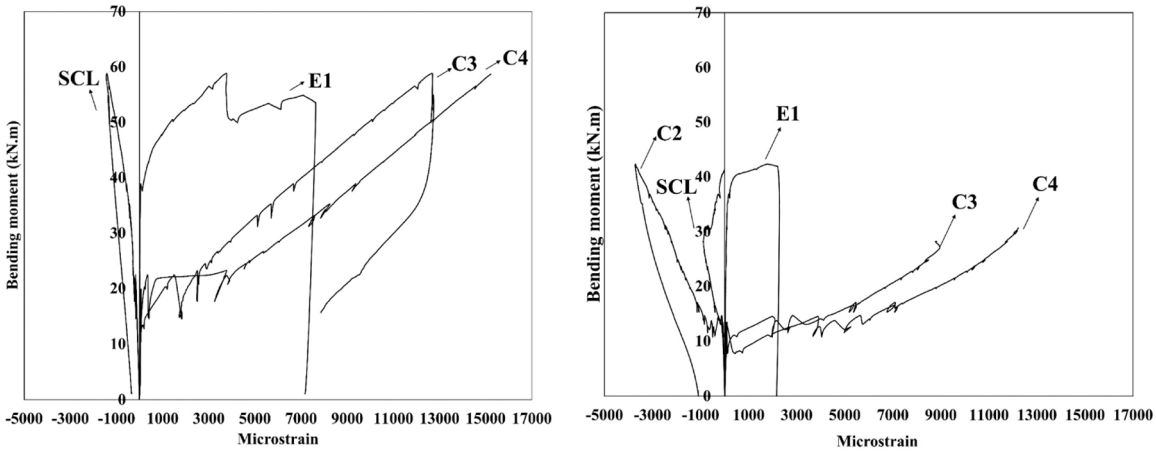

(a) G250L2SB (b) 250L2CB

Fig. 8. Effect of the cutout on moment–strain behavior.

12190 με (57% of ultimate tensile strain), which is significantly higher than the 7190 με (34% of maximum tensile strength) measured in the bars in the solid deck, which indicates that the failure in both decks occurred in the concrete. These results indicate that the wide cracks in the corner of the cutout significantly stressed the longitudinal bars. This strain behaviour supports the shape of the deflection curve reported in

Fig. 7b. While C_3 and C_4 stopped measuring when wide cracks developed in the vicinity of the edge cutout, the strain in E_1 started to increase, reaching up to 2200 $\mu\varepsilon$ due to the propagation of the flexural shear crack in the shear span. This level of strain is less than the typical failure strain in compression for concrete of 3000 $\mu\varepsilon$ which indicates that the deck with an edge cutout failed due to combined shear and flexure. From these results, it can be concluded that the edge cutout initiated the development of a flexural shear crack that exposed the concrete and the GFRP bars to high strain.

3.1.3. Crack propagation and failure behaviour

The discontinuity in deck G250L2CB at the corners of the edge cutout resulted in the concrete cracking developing at a lower bending moment than in G250L2SB. This behaviour can be attributed to the high concentration of stress in the cutout region, which is supported by the high strain measured by C_3 and C_4, as shown in Fig. 8. With the further increase in bending moment (i.e., between 19.7 kN.m and 23.7 kN.m), flexural tensile cracks developed in the solid deck along the constant bending moment region (Fig. 9). At the same time, the uncracked concrete in the compression zone still carried the shear force. This behaviour has been confirmed by Yang et al. [30], who concluded that, in a GFRP-reinforced concrete deck with an opening, the initial crack would typically appear in the region close to the cutout and that the shear crack would extend from the cutout edge to the end of the span. At a bending moment of 39.7 kN.m, an inclined crack formed at the shear span and progressed towards the support. This is supported by the high strain measured by E_1. This shows that the longitudinal GFRP bar was highly stressed and provided dowel action to keep the two concrete segments together. This type of failure is a diagonal tension as also suggested by Kim & Park [31]. At a bending moment of 58.6 kN.m, the failure of the solid deck was due to shear tension, which was observed by Manalo et al. [32] for doubly GFRP-reinforced concrete boat ramp planks.

The initial flexural crack in the cutout region formed in G250L2CB at 13.2 kN.m. After that up to 20 kN.m, hairline cracks developed within the deck's shear span. The first crack at the corner of the edge cutout continued to widen. At a bending moment of 30.6 kN.m, the flexural cracks at the corner of the edge cutout significantly widened and propagated across the deck width, dividing the deck into three segments. At the ultimate bending moment of 42.2 kN.m, significant widening of the crack at the edge cutout reduced the deck's bending moment capacity (Fig. 10). This failure behaviour shows that the pontoon deck with an edge cutout was more prone to more localized concrete cracking than the solid deck. The edge cutout also changed the failure behaviour of the GFRP-reinforced concrete deck from flexural-shear to shear-tension because of the reduced width of the concrete and the discontinuation of the longitudinal GFRP bars in this region.

3.2. Effect of loading span-to-depth ratio

3.2.1. Moment capacity and stiffness

The effect of the span-to-depth ratio on the pontoon deck's flexural behaviour was assessed by comparing the behaviour of decks G250L2CV and G250L2CB. The bending moment behaviour of both decks was similar up to a bending moment of 33.45 kN.m before starting to deviate (Fig. 11). In the pre-cracking stage, the initial stiffness of G250L2CV (12.8 kN/mm) was 34% higher than G250L2CB (9.5 kN/mm). The higher initial stiffness of the deck with a lower span-to-depth ratio was due to the higher loading capacity through the reorientation of the internal force through the arch action of the concrete in the shear span, as also observed by Maranan et al. [11]. In the post-cracking stage, the ultimate bending moment of G250L2CB (42.24 kN.m) was 21% higher than G250L2CV (33.45 kN.m). This higher bending moment can be attributed to G250L2CB (flexural-shear) and G250L2CV (shear-compression) having different failure mechanisms. By considering that both decks have a homogenous cross-section, the maximum shear stress of the uncracked section would be $\tau_{max} = 3V/2A$, where V is the shear force at the uncracked section and A is the uncracked cross-sectional area. Considering a shear crack in the shear span is a diagonal crack between the loading point to the support, the uncracked cross section of G250L2CB was 27.5% higher than G250L2CV, which means that, at the same loading level, the induced stress in G250L2CV was higher and caused shear failure at the lower bending moment. Moreover, at 33.45 kN.m, the induced shear stress in the section of G250L2CB and G250L2CV was 0.8 MPa and 1.08 MPa, respectively. The 25.9% higher shear stress in the deck with a lower span-to-depth ratio (G250L2CV) caused the shear-compression failure to occur in the shear span. Thus, it can be concluded that, at this level of applied load, G250L2CV had reached its concrete shear strength. These results agree with [10], wherein a decrease in the span-to-depth ratio from 1.8 to 1.0 (44% reduction) resulted in the induced shear stress in the section of the solid deck increasing by 28%. This finding also agrees with the results of Abed et al. [33] who found that decreasing the span-to-depth ratio of GFRP-reinforced concrete beams from 1.52 to 1.3 (14.4% reduction) under four-point static loading increased the ultimate shear stress by

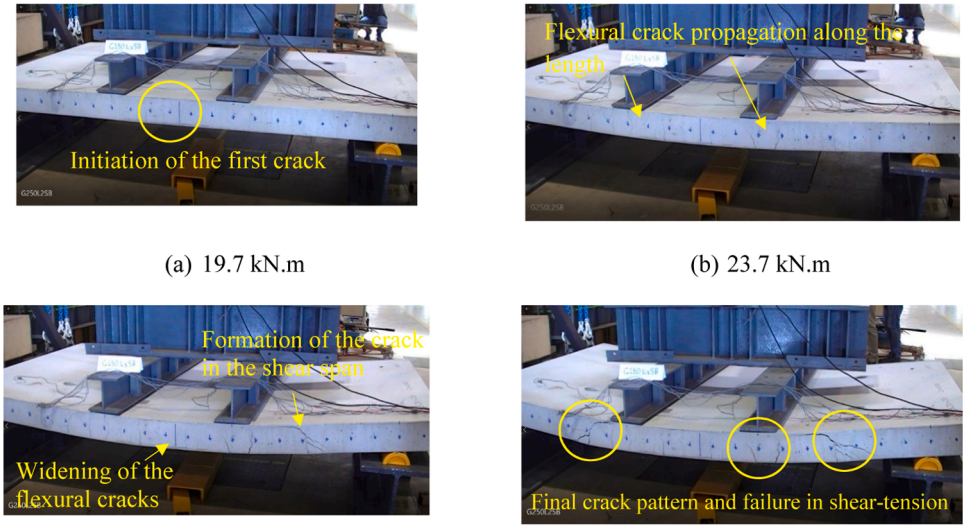

(a) 19.7 kN.m (b) 23.7 kN.m

(c) 39.7 kN.m (d) 58.6 kN.m

Fig. 9. Failure behaviour of G250L2SB.

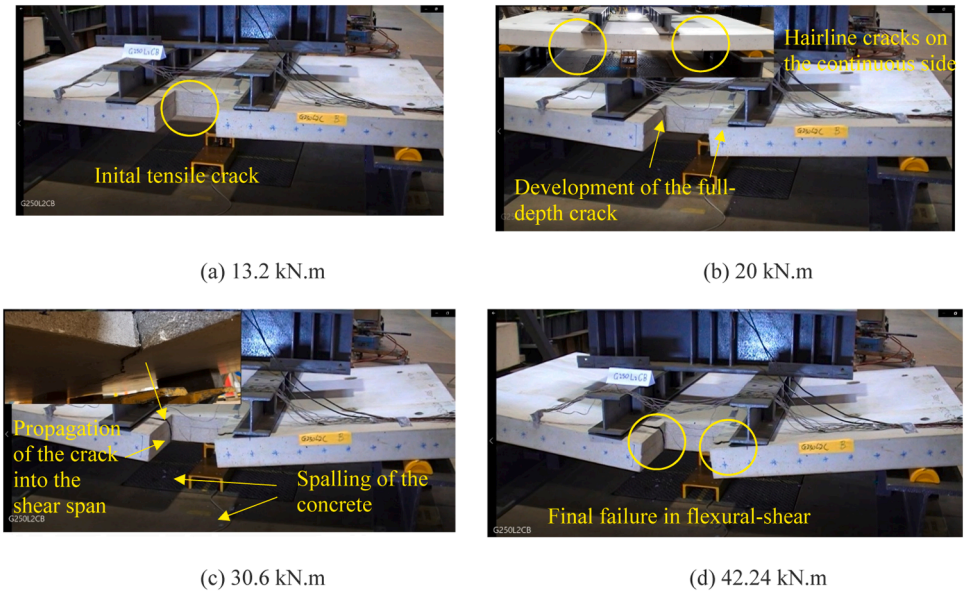

Fig. 10. Failure behaviour of G250L2CB.

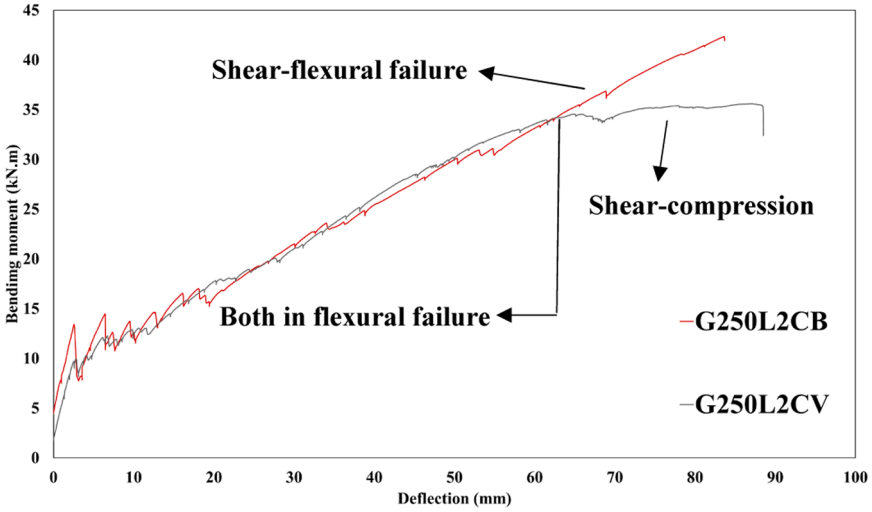

Fig. 11. Effect of the span-to-depth ratio on the moment capacity of the pontoon deck.

10.8%. These observations—which are similar to the effect of the span-to-depth ratio in the solid deck from [10,33] —demonstrate that when the loading point has enough space for the cutout—compressive stress can be developed on the top of the concrete surface, but high shear stress can be induced in the shear span. This caused the development of shear-compression failure, which reduced the overall bending capacity of the deck.

3.2.2. *Moment–strain behaviour*

The span-to-depth ratio for the investigated pontoon decks changed the strain development in the concrete and GFRP bars at applied moments greater than 30 kN.m. This level of bending moment corresponds to the moment at which the strain gauge detached from the mid-span of G250L2CB. The strain in the GFRP bars in tension at mid-span was 12190 $\mu\varepsilon$ and 10474 $\mu\varepsilon$ for G250L2CB and G250L2CV, respectively. The higher strain in G250L2CB was due to the greater curvature of the deck, resulting in a 16% higher strain. On the other hand, the strain at the edge of the bar (E_1) in deck G250L2CV was 11590 $\mu\varepsilon$, which is significantly higher than that of G250L2CB (2229 $\mu\varepsilon$). This can be explained by G250L2CV having a wider crack in its shear span than G250L2CB. To the contrary, G250L2CB had a wider and more concentrated crack pattern between the loading point and cutout than G250L2CV Fig. 12.

3.2.3. *Crack propagation and failure behaviour*

The first crack was observed in both decks in the vicinity of the cutout and both decks exhibited similar cracking propagation up to the applied bending moment of 30 kN.m. After this, G250L2CV had cracks forming in the shear span, while G250L2CB exhibited wide shear cracks at the cutout corner that propagated to the loading point on the bottom surface. The crack propagation at the corner of the cutout in G250L2CB was due to its proximity to the loading point, which created a high concentration of stress. On the other hand, there was a reasonable distance from the loading point to the edge of the cutout in G250L2CV. This reduced the shear span of this deck, however, creating high shear stress at this location. This change in the loading configuration altered the failure behaviour of the deck from flexural-shear for G250L2CB to shear-compression for deck G250L2CV. The crack propagation and failure behaviour are consistent with the results of Al-Fakher et al. [34]. The results of the current study show that the stress concentration and crack development at the edge cutout can be minimized by having the loading

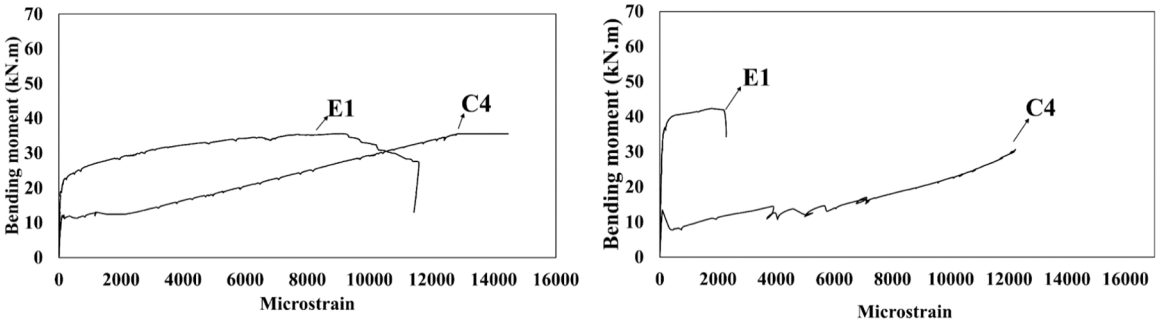

(a) G250L2CV (b) G250L2CB

Fig. 12. Effect of the span-to-depth ratio on the moment–strain behavior.

point far from the corners of the cutout. This, however, will result in a shorter shear span, promoting shear compression failure between the loading point and the support Fig. 13.

3.3. Effect of loading configuration

3.3.1. Load capacity and stiffness

The effect of loading configuration was evaluated by analyzing the bending moment and load–deformation behaviour of decks G250L2CA and G250L2CB. The bending moment values applied by the airbag to the midspan of the deck are calculated by multiplying the pressure applied by the airbags by the width of the sample to simulate the uniform load (in kN/m) and this uniform load is multiplied by the square of the support span (L) divided by 8. Subsequently, applying a uniform load to G250L2CA resulted in 29% and 25% higher initial stiffness and cracking bending moment than under four-point bending in deck G250L2CB. This can be attributed to a more uniform distribution of stress using the airbag. The point load created stress concentration, however, which damaged the concrete surface near the loading point. (Sharda et al. [35] observed similar behaviour for all composite wall panels they studied. The effective bending stress at ultimate for deck G250L2CA was 16.2 MPa, which is 20% higher than the 13.5 MPa for deck G250L2CB (Fig. 14). The higher bending moment exhibited by G250L2CA can also be explained by its lower induced shear stress. The maximum shear stress in deck G250L2CB was 0.64 MPa which is 22% higher than that in G250L2CA (0.52 MPa). This shows that the deck under four-point loading (G250L2CB) experienced combined flexural and shear stress, while G250L2CA had minimal shear stress.

3.3.2. Moment–strain behaviour

In both loading scenarios (four-point and uniform loading), the strain in the GFRP bars at the tension zone and the mid-span had a steep first slope (pre-cracking stage), a second plateaued stage, and a third stage with a slope lower than the first part (post-cracking stage), as shown in Fig. 15. The measured strain in the pre-cracking stage increased linearly by 13.2 and 19.2 kN.m in G250L2CB and G250L2CA, respectively. That corresponds to the deck's cracking moment and supports the deck's moment behaviour. The second and third stages signify the deck's nonlinear behaviour, indicating crack widening and propagation at the mid-span. The measured strain in both the concrete and GFRP bars in deck G250L2CA was lower than in G250LCB at the same level of bending moment. This shows that the concrete and the GFRP bars loaded uniformly were better at resisting the applied load together up to failure than under point loading. This is because of the more uniform cracking propagation and narrower crack under the uniform distribution of the load. The wider cracks in deck G250LCB transferred most of the strain to the GFRP bars. This meant that deck G250L2CA made better use of the high tensile strength and strain of the GFRP bars than G250L2CB in which the strain recorded in the GFRP bars reached 47.5% of its ultimate strain. Compared to deck G250LCB, the measured strain in the GFRP bars in G250L2CA was 58% of its ultimate.

3.3.3. Cracking propagation and failure behaviour

The cracking propagation and failure behaviour of the GFRP-reinforced concrete pontoon decks were very different under uniform and four-point loading (Fig. 16). Initial flexural cracks were formed in the vicinity of the cutout at the tension zone of both G250L2CB and G250L2CA. However, increasing the applied uniform loading with airbags caused the deck (G250L2CA) to exhibit flexural and compressive compression of the concrete. On the other hand, the application of the concentrated load under four-point loading resulted in the deck (G250L2CB) having flexural-shear behaviour.

3.4. Effect of reinforcing arrangement

3.4.1. Moment capacity and stiffness

The impact of the reinforcement arrangement on the moment capacity and stiffness of the GFRP-reinforced concrete pontoon decks were evaluated by comparing the behaviour of G150L1CA (single layer) and G250L2CA (double layer) (Fig. 17).

The results show that G250L2CA had 25.3% higher initial stiffness (12.69 kN/mm compared to 9.47 kN/mm), 27.7% higher cracking

(a) 30 kN.m (b) 33.45 kN.m

Fig. 13. Failure behaviour of G250L2CV.

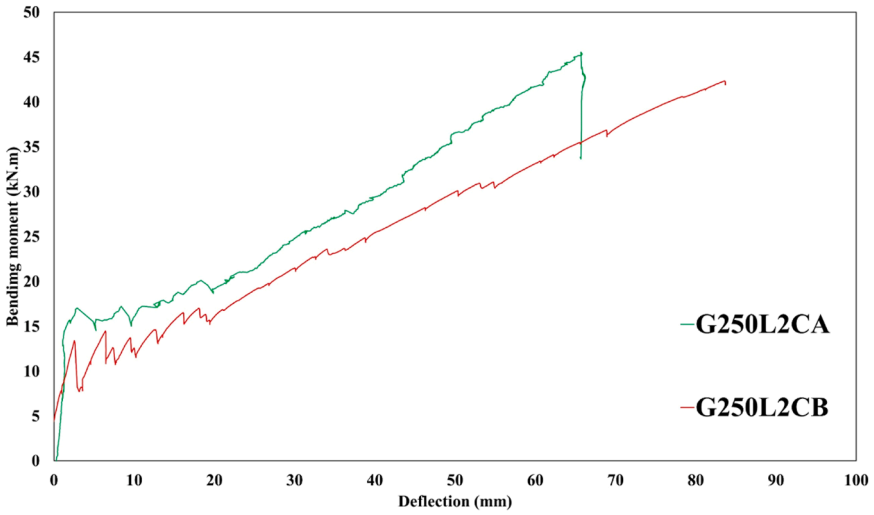

Fig. 14. Effect of the loading configuration on the moment capacity of the pontoon deck.

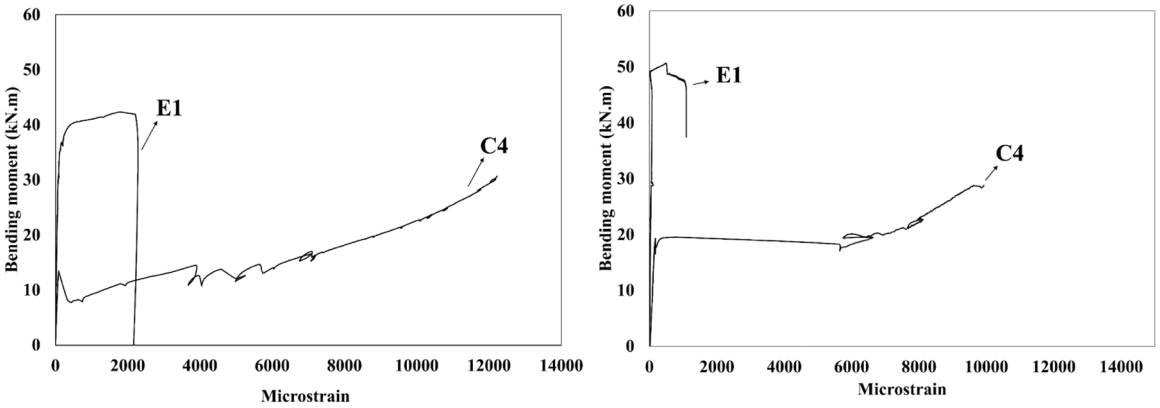

Fig. 15. Effect of the loading configuration on moment–strain behavior.

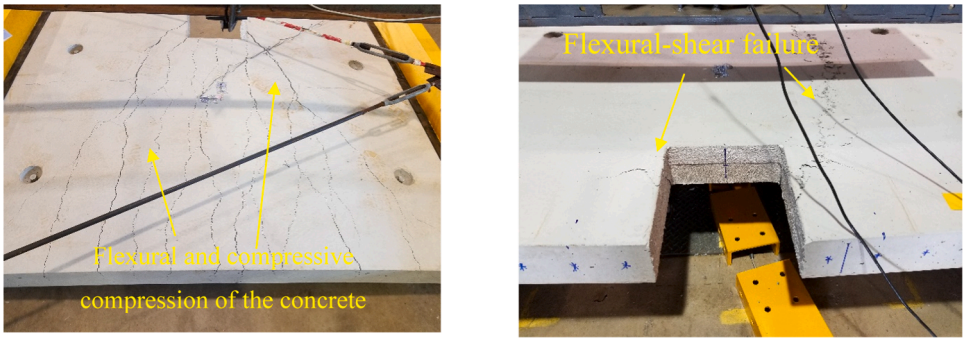

Fig. 16. Effect of the loading condition on failure behavior.

moment (13.8 kN-m compared to 19.1 kN-m) and 25.6% higher bending moment capacity (37.6 kN-m compared to 50.6 kN-m) than G150L1CA. This can be explained by deck G250L2CA having a higher effective depth (36.6%) than G150L1CA and the neutral axis in G150L1CA from the top fibre in compression is (10.27 mm) and in G250L2CA (14.29 mm), in which the longitudinal reinforcement of G250L2CA was more effective in helping the bottom concrete to resist tension. This can also be attributed to the dowel action of the longitudinal reinforcement and aggregate interlocking being lower when the GFRP bars were at deck mid-depth. In that case, only the concrete above the longitudinal bars would be resisting uniform loading. Moreover, increasing the effective depth enabled the tensioned GFRP bars to contribute to higher

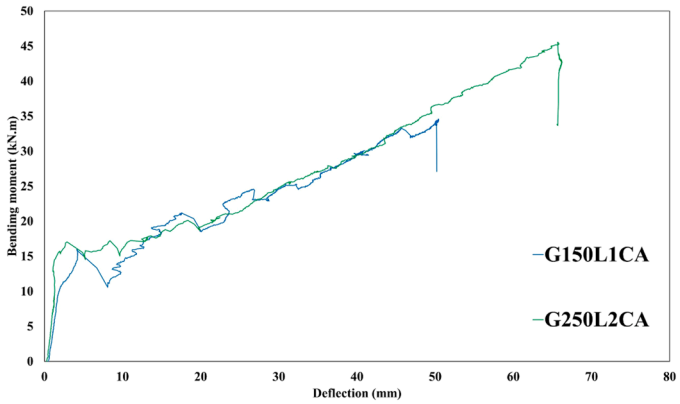

Fig. 17. Moment-deflection curve of the pontoon deck with different reinforcing arrangements.

continuity within the concrete section. Compared to the solid boat ramp plank investigated by [32], these decks achieved slightly lower improvement in the cracking moment when the effective depth increased. The edge cutout in the decks investigated in this study could account for that.

3.4.2. Moment–strain behaviour

The results indicate that regardless of the number of GFRP reinforcement layers, trilinear strain behaviour occurred at deck mid-span, as reported in [32,36]. After initiation of the first crack and the strain in the gauge C_3 during the nonlinear stage, the plateau part continued to increase until 2075 $\mu\varepsilon$ (9.8% of the ultimate tensile strain) and 6480 $\mu\varepsilon$ (30.8% of the maximum tensile strength) in G150L1CA and G250L2CA, respectively, which means increasing the effective depth allowed the tensioned GFRP bars to perform more efficiently along the length of the deck in preventing cracks from forming and widening (Fig. 18).

Although past studies [32,36] found similar strain patterns in solid slabs, an analysis of the values recorded by the gauges attached to the tensioned GFRP bar in the G250L2CA revealed notable differences. Specifically, comparing the strain measured by two gauges revealed that the one closer to the cutout had a significantly higher strain. This suggests that the crack, which was wider due to concentrated stress, propagated from the corner edge of the cutout. Based on these results—and as predicted—increasing the effective depth at the same level of loading, exposed the GFRP bars to higher strain and helped impede the propagation of flexural cracks.

3.4.3. Failure behaviour

Regardless of the arrangement of the GFRP bars, the cracks in both decks initiated from the corners of the cutout. The failure mechanism of both decks was due to the flexural cracks and crushing of the concrete in compression. The cracks in the single-layer reinforced deck were significantly wider than that of the deck reinforced with two layers of GFRP bars. In G250L2CA, the cracks were narrow and distributed on the surface of the deck as the tensile GFRP bars were closer to the top concrete surface, thereby resisting the opening of the flexural cracks

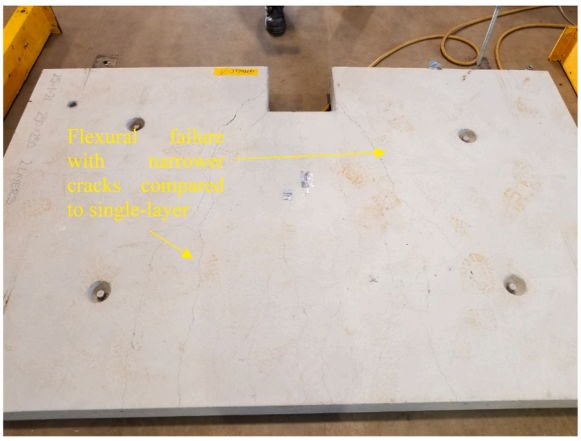

(a) G250L2CA

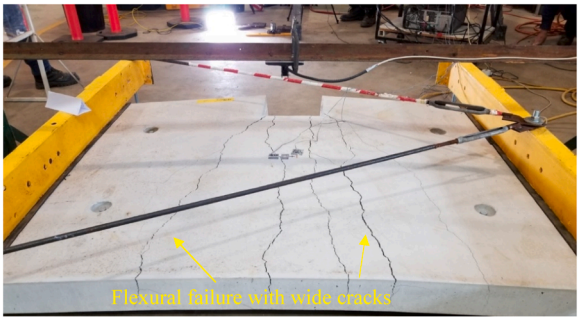

(b) G150L1CA

Fig. 19. Effect of the reinforcing arrangement on failure behavior.

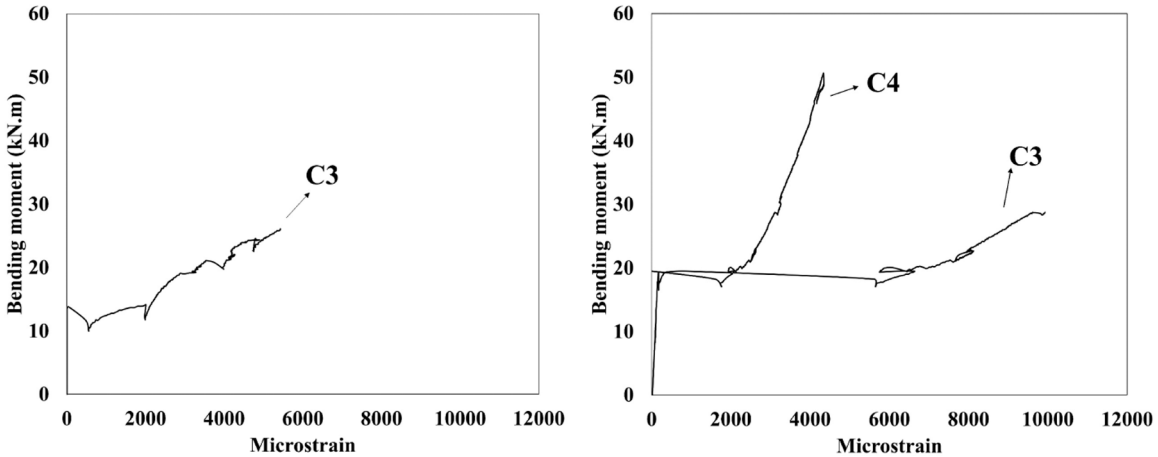

(a) G150L1CA (b) G250L2CA

Fig. 18. Effect of the reinforcing arrangement on the moment–strain behavior.

Table 4
Comparison of theoretical evaluation and experimental results.

Specimen	(M_{cr}, M_u, V_c)		
	Experimental value	CSA S806-12[37]	ACI 440.1R-15[38]
G150L1CA	(14.6, 39.1, 80.9)	(16, 36.7, 37.8)	(16.6, 35.1, 40.7)
G250L2CA	(19.1, 50.9, 106.2)	(16, 47.3, 36.6)	(16.6, 46.5, 40)
G250L2CB	(13.2, 42.2, 59.5)	(16, 47.3, 36.6)	(16.6, 46.5, 40)
G250L2SB	(19.7, 58.6, 83.9)	(20, 59.1, 45.7)	(20.7, 58.1, 50)
G250L2CV	(10.1, 35.4, 70.5)	(16, 47.3, 36.6)	(16.6, 46.5, 40)

(Fig. 19a). Less dowel action and aggregate interlock induced by a low effective depth of the GFRP bars in tension in deck G150L1CA provided limited control of flexural cracks propagating and widening (Fig. 19b). A comparison of the results reveals that the impact of effective depth is consistent with the observations made by Manalo et al. [36] in the case of solid slabs. Nevertheless, there was a distinct difference in the location of crack initiation between the solid deck and the deck with a cutout. While tensile cracks initially formed in the mid-span of the solid deck, the initial crack in the deck with a cutout occurred solely at the edge of the cutout. It is however recommended that in the future experimental program, the crack width and crack spacing data can further support the analyses of the synergistic forces between GFRP reinforcement and concrete.

4. Theoretical evaluation and comparison with experimental DATA

The cracking (M_{cr}) and the ultimate bending moment (M_u), as well as the shear capacity (Vc) of the GFRP-reinforced decks, were calculated using the equations recommended in (CSA S806–12 [37]) and (ACI 440. R-15 [38]) (Table 4). The material factors, such as λ and φ_c, were assumed to be equal to 1.0 as was also implemented in [10]. Moreover, the minimum width at the middle of the deck was considered in calculating the behaviour of the solid specimen (1500 mm) and those with an edge cutout (1200 mm). Engineering characterization parameters for the concrete and GFRP bars (namely, modulus of elasticity, compressive strength of concrete, and dimensions) are reported in the experimental program (Tables 2 and 3). Other assumptions to determine the value of α_1 and β_1 are listed (Table 5). CSA S806–12 [37] (0.0035) typically assumes a higher value of $\varepsilon_{cu}^{'}$ than ACI 440.1R-15 [38] (0.003). The contribution of the reinforcement bars in the compression zone was not considered for decks with a double layer of reinforcement. In general, the shear resistance of the pontoon decks consisted of a combination of various mechanisms, including the uncracked concrete, aggregate interlocking, dowel action, and arch action which applied to the concrete deck with span-to-depth ratio below 2.5 [31,34]. In both reinforcement arrangements, the reinforcement ratio and balanced reinforcement ratio can be obtained from Eqs. 1–2.

$$\rho_f = \frac{A_f}{bd} \tag{1}$$

$$\rho_{fb} = 0.85\beta_1 \frac{f_c^{'}}{f_{fu}} \frac{E_f \varepsilon_{cu}}{E_f \varepsilon_{cu} + f_{fu}} \tag{2}$$

Since this study considered the concrete strength and longitudinal reinforcement ratio (except for G150L1CA) to be similar for all the tested specimens, the effect of all shear mechanisms except arch-action was assumed to be identical. Moreover, in all specimens, the reinforcement ratio is higher than the balanced reinforcement ratio (0.45%) and the position of the neutral axis can be determined from the strain and stress distribution, and internal forces in the cross-section

Table 5
CSA S806–12 and ACI 440.1R-15 prediction equations.

CSA S806-12[37]	ACI 440.1R-15[38]
$M_{cr} = f_r \times \frac{I_g}{y_t}$ (3)	
$f_r = 0.6\lambda\sqrt{f_c^{'}}$ (4)	$f_r = 0.62\lambda\sqrt{f_c^{'}}$ (6)
$M_u = \rho_f f_f b d^2 \left(1 - \frac{\rho_f f_f}{2\alpha_1 f_c^{'}}\right)$ (5)	$M_u = \rho_f f_f b d^2 \left(1 - 0.59\frac{\rho_f f_f}{f_c^{'}}\right)$ (7)
$f_f = \frac{\varepsilon_{cu}(d-c)}{c} E_f < f_{fu}$ (8)	$f_f = \sqrt{\frac{(E_f \varepsilon_{cu})^2}{4} + \frac{0.85\beta_1 f_c^{'}}{\rho_f} E_f \varepsilon_{cu}} - 0.5 E_f \varepsilon_{cu} < f_{fu}$ (9)
	$\alpha_1 = 0.85 - 0.0015 f_c^{'} \geq 0.67$ $\beta_1 = 0.85 - 0.0025 f_c^{'} \geq 0.67$ (Eqs. 10-11)
	$\alpha_1 = 0.85$ $\beta_1 = 0.85 - \frac{0.05(f_c^{'} - 27.6)}{6.9} \geq 0.67$ (Eqs. 12-13)
$V_c = 0.05\lambda\phi_c k_m k_r \sqrt[3]{f_c^{'}} b d_v$ (14)	$V_c = \frac{2}{5}\sqrt{f_c^{'}} b c$ (15)
	$k_m = \sqrt{\frac{V_f d}{M_f}} \leq 1$ $k_r = 1 + \sqrt[3]{E_{fv}\rho_{fv}}$ (Eqs. 16-18) $d_v = kd \geq \max[0.9d, 0.72h]$
	$k = \sqrt{2\rho_{fc} n_f + (\rho_{fc} n_f)^2} - \rho_{fc} n_f$ (Eqs. 19-20)

($0.85f_c^{'}b\beta_1 c = A_f f_f$) which f_f can be determined by ($f_f = E_f \varepsilon_{cu} \frac{\beta_1 d - \beta_1 c}{\beta_1 c}$) (ACI 440. 1R-15 [38]).

The flexural strength of a solid deck with a double layer (G250L2SB) in terms of cracking and ultimate bending moment was accurately estimated by the prediction equations as indicated by comparison with the experimental values. The cracking moment of G250L2CB and G250L2CS, however, was lower than predicted, owing to the edge cutout, which caused a crack to form at a relatively lower bending moment. Given the cutout (G250L2CB) and the stress concentration at its corners, the ultimate bending moment of the experimental value was 10.8% lower than the predicted value. In contrast to these and on average, the experimental cracking ultimate bending moment of G250L2CA was 17.1% and 8.5% higher than their predicted values based on CSA and ACI equations, respectively. This is likely due to the evenly distributed load on the deck surface and the absence of any stress concentration in uniform loading distribution, resulting in improved deck flexural performance. This was observed in G150L1CA. The ultimate bending moment capacity of the experimental specimen was 8.7% higher, but the cracking moment was, on average, 10.4% lower than predicted. This can be attributed to the greater distance between the concrete surface and the GFRP bars, resulting in crack formation near the cutout at a lower bending moment. As predicted, both equations conservatively predicted the shear strength of the GFRP-reinforced concrete pontoon decks. Of the design equations in the study, the CSA S806–12 [37] equation gave more conservative estimates of the shear capacity of the GFRP-reinforced deck, as observed in [40]. The average ratio between the predicted and experimental shear strength was 0.49, which is lower than with the ACI 440.1R-15 [38] equation (0.54). This latter value is quite comparable to the specimen studied by Maranan et al. [40] without stirrups and with a higher span-to-depth ratio of 0.51. The other specimens tested in [10] involved stirrups and as predicted, the ratio was higher. This evaluation shows that the current equations in the standards reliably describe the shear and flexural behaviour of GFRP-reinforced concrete decks with or without an edge cutout and with the design parameters investigated in this study.

5. Conclusion

This experimental study investigated the flexural behaviour of GFRP-RC pontoon decks under static uniform and four-point loading conditions. The effect of the cutout, span-to-depth ratio, and effective depth on the moment capacity, strain behaviour, and failure mechanism of the decks was evaluated. The following conclusions can be drawn from the findings of this study:

- The presence of a square cutout on the deck's edge reduced the flexural behaviour of the deck by 10% due to lower bending stress and changed the failure behaviour from shear tension to flexural shear, causing the deck to fail as a result of excessive cracks initiated from the cutout corner. This behaviour arises from stress concentration in the sharp corner of the square cutout, which can be mitigated with the use of a circular cutout.
- The span-to-depth ratio (a/d) considered has no effect on the pre-cracking and post-cracking responses of the decks. Decreasing the a/d, however, increased the induced shear stress of a section, changing the failure mechanism from flexural shear cracking to shear compression failure.
- The bending stress at failure is higher by 20% for uniform loading compared to four-point loading due to the even load distribution and the absence of stress concentration around the loading point. Under four-point loading, the deck failure mechanism changed from flexural and compression crushing of the concrete to flexural shear.
- An increase in effective depth led to improvements in all of the decks' flexural characteristics Although the failure of the tested specimens was similar, the mechanism associated with double-layered reinforcement meshes can be attributed to slower crack propagation in the post-cracking stage.
- The moment-carrying capacities of the solid deck in both the pre-and post-cracking stages were reasonably estimated with the ACI-440.1R-15 and CSA S806-12. The presence of a cutout and higher potential for crack formation and extension resulted in the prediction equations in both codes overestimating the flexural capacity of the decks under four-point bending by 10%. However, the experimental outcomes were higher than expected when the deck was subjected to uniform loading.

Additional investigations are suggested to consider other important design parameters that may affect the structural behavior of GFRP-reinforced pontoon decks including the shape of the cutouts, type and surface profiles of the reinforcing bars to refine the design procedures. This will help achieve a safer, more resilient and efficient concrete pontoon decks.

Declaration of Competing Interest

The authors would like to declare and confirm that there is no conflict of interest of this manuscript.

Acknowledgements

The authors would like to express their special appreciation to the Advance Queensland Industry Research Fellowship Program (AQIRF 119-2019RD2) and the Cooperative Research Centre Project (CRCPXIII000007) for its financial support and to Sustainable Alliance Pty Ltd for supplying the GFRP reinforcements. The authors are grateful to The Jetty Specialist for fabricating the precast-concrete pontoon decks and for the assistance from technicians and students at the University of Southern Queensland.

References

[1] Nolan S, Rossini M, Knight C, Nanni A. New directions for reinforced concrete coastal structures. J Infrastruct Preserv Resil 2021;2(1):1–12.
[2] Manalo AC, Mendis P, Bai Y, Jachmann B, Sorbello CD. Fiber-reinforced polymer bars for concrete structures: State-of-the-practice in Australia. J Compos Constr 2021;25(1):05020007.
[3] Shayan, A., & Xu, A. (2016). Realizing 100-year bridge design life in an aggressive environment: review of the literature.
[4] Zhou C, Pan J, Zhang Z, Zhu Y. Comparative study on the tensile mechanical behaviour of GFRP bars under and after high-temperature exposure. Case Stud Constr Mater 2022;16:e00905.
[5] Khatibmasjedi M, Ramanathan S, Suraneni P, Nanni A. Durability of commercially available GFRP reinforcement in seawater-mixed concrete under accelerated aging conditions. J Compos Constr 2020;24(4).
[6] Manalo A, Maranan G, Benmokrane B, Cousin P, Alajarmeh O, Ferdous W, et al. Comparative durability of GFRP composite reinforcing bars in concrete and in simulated concrete environments. Cem Concr Compos 2020;109:103564.
[7] Ramanathan S, Benzecry V, Suraneni P, Nanni A. Condition assessment of concrete and glass fiber reinforced polymer (GFRP) rebar after 18 years of service life. Case Stud Constr Mater 2021;14:e00494.
[8] Mufti, A., Onofrei, M., Benmokrane, B., Banthia, N., Boulfiza, M., Newhook, J., et al. "Durability of GFRP Reinforced Concrete in Field Structures." Proceedings of the 7th International Symposium on Fibre Reinforced Polymer (FRP) Reinforcement for Concrete Structures (FRPRCS-7), Kansas City, 2005. pp. 1361–1378.
[9] Akbari Hadad H, Nanni A. Fatigue behaviour of FRCM-strengthened RC beams. J Compos Constr 2020;24(6).
[10] Maranan GB, Manalo AC, Benmokrane B, Karunasena W, Mendis P, Nguyen TQ. Shear behaviour of geopolymer-concrete beams transversely reinforced with continuous rectangular GFRP composite spirals. Compos Struct 2018;187:454–65.
[11] Maranan GB, Manalo AC, Benmokrane B, Karunasena W, Mendis P, Nguyen TQ. Flexural behaviour of geopolymer-concrete beams longitudinally reinforced with GFRP and steel hybrid reinforcements. Eng Struct 2019;182:141–52.
[12] Ifrahim MS, Sangi AJ, Ahmad SH. Experimental and numerical investigation of flexural behaviour of concrete beams reinforced with GFRP bars. Structures 2023;56:104951. Elsevier.
[13] Hassanli R, Vincent T, Manalo A, Smith ST, Gholampour A, Gravina R. Large-scale experimental study on pocket connections in GFRP-reinforced precast concrete frames. Structures 2021;34:523–41. Elsevier.

[14] Zhou L, Zheng Y, Di B, Lv J, Taylor SE. Shear behaviour of SWSS-SCC beams reinforced with GFRP bars and stirrups: experimental and analytical investigations. Structures 2023;56:104946. Elsevier.
[15] Manalo A, Alajarmeh O, Yang X, Ferdous W, Ebrahimzadeh S, Benmokrane B, et al. Development and mechanical performance evaluation of a GFRP-reinforced concrete boat-approach slab. Structures 2022;46:73–87. Elsevier.
[16] Al-Rousan RZ. Impact of elevated temperature on the behavior of full-scale concrete bridge deck slabs reinforced with GFRP bars. Structures 2022;43:621–34. Elsevier.
[17] Wang J, Cheng B, Yan X, Zhang K, Zhou Z. Structural analysis and optimization of an advanced all-GFRP highway bridge. Structures 2021;34:3155–71. Elsevier.
[18] Standard, A. (2015). Design Criteria for Floating Walkways and Pontoons, Transport and Main Roads, October 2015, State of Queensland (Department of Transport and Main Roads), Australia [Online] Available on: Error. Hyperlink reference not valid. n_of_marinas. pdf. Accessed: April, 4, 2020.
[19] Australian Standards AS3600:2018, Concrete Structures. Standards Australia Limited, Sydney, New South Wales 2001, Australia.
[20] Lu J, Afefy HM, Azimi H, Sennah K, Sayed-Ahmed M. Bond performance of sand-coated and ribbed-surface glass fiber reinforced polymer bars in high-performance concrete. Structures 2021;34:10–9. Elsevier.
[21] Arias JPM, Vazquez A, Escobar MM. Use of sand coating to improve bonding between GFRP bars and concrete. J Compos Mater 2012;46(18):2271–8.
[22] AlAjarmeh OS, Manalo AC, Benmokrane B, Karunasena W, Mendis P, Nguyen KT. Compressive behaviour of axially loaded circular hollow concrete columns reinforced with GFRP bars and spirals. Constr Build Mater 2019;194:12–23.
[23] DTMR, 'Transport and Main Roads Specifications MRTS70 Concrete', Transport and Main Roads Specifications, 2018.
[24] AS 3972. (2010). General purpose and blended cements. Standards Australia.
[25] Standard, A. (2007). AS 1379—2007. Specification and supply of concrete. Australian Standard, Sydney, NSW, Australia.
[26] Standards Australia. (2014). Aggregates and rock for engineering purposes, concrete aggregates (No. AS 2758.1, pp. 1–32). Sydney.
[27] ASTM, A. (2018). ASTM C39/C39M-18 standard test method for compressive strength of cylindrical concrete specimens. ASTM International, West Conshohocken, PA. ASTM, AI (2018)." ASTM C, 192.
[28] Khalil AEA, Atta AM, Hassan A, Abd-Elaaty AH. Flexural strength recovery of RC one-way slabs having cut-outs using NSM-SHCC plates. Eng Struct 2022;258:114149.
[29] Salman WD. Strengthening of reinforced concrete one-way slabs with opening using CFRP strip in flexural. Int J Sci Res 2015;4:4–438.
[30] Yang X, Alajarmeh O, Manalo A, Benmokrane B, Gharineiat Z, Ebrahimzadeh S, et al. Torsional behaviour of GFRP-reinforced concrete pontoon decks with and without an edge cutout. Mar Struct 2023;88:103345.
[31] Kim, J.K., & Park, Y.D. (1996). Prediction of shear strength of reinforced concrete beams without web reinforcement. American Concrete Institute.
[32] Manalo AC, Alajarmeh O, Cooper D, Sorbello CD, Weerakoon SZ, Benmokrane B. Manufacturing and structural performance of glass-fiber-reinforced precast-concrete boat ramp planks. Structures 2020;28:37–56. Elsevier.
[33] Abed F, El-Chabib H, AlHamaydeh M. Shear characteristics of GFRP-reinforced concrete deep beams without web reinforcement. J Reinf Plast Compos 2012;31(16):1063–73.
[34] Al-Fakher U, Manalo A, Ferdous W, Alajarmeh O, Aravinthan T, Zhuge Y, et al. Shear behaviour of hollow precast concrete-composite structures. Mater Struct 2021;54:1–18.
[35] Sharda A, Manalo A, Ferdous W, Bai Y, Nicol L, Mohammed A, et al. Flexural behaviour of composite modular wall systems under uniformly distributed and concentrated loads. Compos Struct 2022:116346.
[36] El-Nemr A, Ahmed EA, El-Safty A, Benmokrane B. Evaluation of the flexural strength and serviceability of concrete beams reinforced with different types of GFRP bars. Eng Struct 2018;173:606–19.
[37] Design, C.S.A. (2012). Construction of Building Structures with Fibre-Reinforced Polymers (CAN/CSA8061 S–S2). Canadian Standards Association: Mississauga, ON, Canada.
[38] American Concrete Institute. Guide for the design and construction of structural concrete reinforced with fiber-reinforced polymer (FRP) bars. (ACI 440.1 R-15). Farmington Hills, Michigan: American Concrete Institute; 2015.
[39] Standard, A. S. T. M. D7205/D7205M-06 (*2011*). Standard test method for tensile properties of fiber reinforced polymer matrix composite bars. ASTM D7205/D7205M-06, ASTM International, West Conshohocken, Philadelphia, Pa 19103.
[40] Maranan GB, Manalo AC, Benmokrane B, Karunasena W, Mendis P. Shear behaviour of geopolymer concrete beams reinforced with glass fiber-reinforced polymer bars. ACI Struct J 2017;114(2).